中国光学 Chinese Optics 核心期刊

电场中Sm原子的第一电离阈移动

许照锦 张小虎 张文纳 黄朝宏 沈礼

Shift of the first ionization threshold of Sm atom in electric field

XU Zhao-jin, ZHANG Xiao-hu, ZHANG Wen-na, HUANG Chao-hong, SHEN Li

引用本文:
许照锦, 张小虎, 张文纳, 黄朝宏, 沈礼. 电场中Sm原子的第一电离阈移动[J]. 中国光学, 2020, 13(6): 1385-1400. doi: 10.37188/CO.2020-0071
XU Zhao-jin, ZHANG Xiao-hu, ZHANG Wen-na, HUANG Chao-hong, SHEN Li. Shift of the first ionization threshold of Sm atom in electric field[J]. *Chinese Optics*, 2020, 13(6): 1385-1400. doi: 10.37188/CO.2020-0071

在线阅读 View online: https://doi.org/10.37188/CO.2020-0071

您可能感兴趣的其他文章

Articles you may be interested in

氢原子在少周期强激光场中阈上电离的电子波包干涉图像

Electron wave packet interference images in above-threshold ionization of hydrogen atoms by few-cycle intense laser fields

中国光学. 2019, 12(6): 1376 https://doi.org/10.3788/CO.20191206.1376

基于第一性原理的钙钛矿材料空位缺陷研究

Investigation of self-doping in perovskites with vacancy defects based on first principles

中国光学. 2019, 12(5): 1048 https://doi.org/10.3788/CO.20191205.1048

用于超冷原子囚禁的一体式结构三维光晶格系统

The integrated three dimensional optical lattice system for confining ultra-cold atoms

中国光学. 2019, 12(6): 1295 https://doi.org/10.3788/CO.20191206.1295

瓦级319nm单频连续紫外激光的实现及铯原子单光子Rydberg激发

Realization of a watt-level 319-nm single-frequency CW ultraviolet laser and its application in single-photon Rydberg excitation of cesium atoms

中国光学. 2019, 12(4): 701 https://doi.org/10.3788/CO.20191204.0701

范围限制的自适应亮度保持多阈值直方图均衡算法研究

Range limited adaptive brightness preserving multi-threshold histogram equalization algorithm

中国光学. 2017, 10(6): 726 https://doi.org/10.3788/CO.20171006.0726

纳米尺度下的局域场增强研究进展

Advances in the local field enhancement at nanoscale

中国光学. 2018, 11(1): 31 https://doi.org/10.3788/CO.20181101.0031

文章编号 2095-1531(2020)06-1385-16

Shift of the first ionization threshold of Sm atom in electric field

XU Zhao-jin, ZHANG Xiao-hu, ZHANG Wen-na, HUANG Chao-hong, SHEN Li*
(*School of Science*, *Tianjin University of Technology*, *Tianjin* 300384, *China*)
* *Corresponding author*, *E-mail*: *shenli@tjut.edu.cn*

Abstract: In order to obtain the first ionization threshold of Sm atom, the photoionization signal, autoionization signal and field ionization signal generated by the Sm atom under multi-step excitation were distinguished, and the influence of the Rydberg state of the Sm atom with different magnetic quantum numbers on the first ionization threshold was studied. At first, by use of multi-step resonance excitation combined with polarization technology, the rare-earth Sm atoms were excited to the autoionization or bound Rydberg state with a specific magnetic quantum number near the first ionization threshold. Then the ions generated by photoionization and autoionization were pushed out of the action zone by the reverse electrostatic field, and a delayed pulsed electric field was applied to detect the Sm atoms of bound Rydberg state. Finally, the relationship between the first ionization threshold of Sm atom and the varying intensity of electrostatic field was acquired, and the first ionization threshold of the Sm atom with different magnetic quantum numbers under zero field was determined by fitting. The experimental results show that the first ionization threshold of Sm atom is 45 519.69±0.17 cm^{-1}, which has been compared with the results obtained by other methods. The effectiveness of the delayed field ionization technique in measuring the first ionization threshold of Sm atom has been verified.

Key words: photoionization; field ionization; first ionization threshold; Sm atom; spectra of highly excited state

收稿日期:2020-04-21; **修订日期**:2020-05-27

基金项目:国家自然科学基金青年科学基金项目(No. 11604243);天津市高等学校创新团队培养计划项目(No. TD3-5029);国家级大学生创新创业训练计划资助项目(No. 201810060026)

Supported by National Natural Science Foundation of China (No. 11604243); Program for Innovative Research Team in University of Tianjin (No. TD3-5029); National Undergraduate Training Programs for Innovation and Entrepreneurship (No. 201810060026)

电场中 Sm 原子的第一电离阈移动

许照锦，张小虎，张文纳，黄朝宏，沈　礼*
（天津理工大学 理学院，天津 300384）

摘要：为了获得 Sm 原子的第一电离阈，将 Sm 原子多步激发产生的光电离、自电离和场电离信号进行了区分，并研究了不同磁量子数 Rydberg 态 Sm 原子对第一电离阈的影响。首先，结合多步共振激发和偏振组合技术，将稀土 Sm 原子激发到第一电离阈附近具有特定磁量子数的自电离或束缚 Rydberg 态。接着，通过反向静电场将光电离和自电离等过程产生的离子推出作用区。然后，通过施加延时脉冲电场对束缚 Rydberg 态 Sm 原子进行探测。最后，通过改变静电场强度获得了 Sm 原子第一电离阈随着静电场强度的变化情况，拟合确定了零场下不同磁量子数 Sm 原子的第一电离阈。实验结果表明：Sm 原子的第一电离阈为 45 519.69±0.17 cm^{-1}；该结果与用其它方法获得的结果进行了比较。实验验证了延时场电离探测技术用于测量 Sm 原子第一电离阈的有效性。

关　键　词：光电离；场电离；第一电离阈；Sm 原子；高激发态光谱
中图分类号：O433.1;O433.2　　**文献标志码：**A　　**doi:** 10.37188/CO.2020-0071

1　Introduction

The first ionization threshold is one of the most important atomic characteristic parameters that determine the chemical properties of elements[1-2]. The precise measurement of the first ionization threshold is very helpful for understanding the electronic structure and chemical properties of an element[3]. For heavy elements, not only Coulomb interaction but also electron-electron correlation, quantum electrodynamics and relativistic effect need to be considered, which makes it very difficult to accurately measure the first ionization threshold of a heavy element[1, 3-5]. Generally, the first ionization threshold is measured by resonance ionization mass spectrometry[1], Rydberg energy-level convergence[6-7], surface ionization[8], electric-field ionization threshold shift[9] and other methods.

As far as the heavy elements (such as lanthanide rare earth atom) are concerned, most of them have an unfilled 4f subshell, and their highly excited state may contain the transitions of both the outermost electron and the 4f subshell electron, so that their spectra are very complex [5, 10-15]. This is especially true for Sm atom. Since there are 6 metastable states of Sm atom, namely $4f^6 6s^2\ ^7F_J$ (J = 1-6), above the ground state $4f^6 6s^2\ ^7F_0$, these metastable states will also have a population when the Sm metal is heated to prepare atomic samples. This leads to a variety of possibilities for the initial state of Sm atom. Moreover, a Sm atom has 8 valence electrons, which makes it possible to have a large number of atomic states in the same electron configuration and then the extreme complexity of energy level structure of Sm atom. In short, these characteristics of Sm atom make its atomic spectrum more challenging than those of other rare earth atoms[16-19]. Similar to Yb atom[20], Ho atom[21] and Eu atom[9] in the rare earth family and Ba atom[22] in the alkaline earth family, Sm atom also has a very wide autoionization peak near the first ionization threshold due to the increased probability of collisions between the atoms in highly excited Rydberg state converging to the first ionization threshold. As a result, it is difficult to directly determine the first ionization threshold, which can be obtained only by using the Rydberg-Ritz formula to fit the energy level data in the Rydberg series[6-7, 21]. However, due to the complexity of multi-step excitation and atomic energy

levels, some interference levels in the non-Rydberg series, in addition to the energy levels in the Rydberg series, also appear in the spectrum of high excited state and increase the uncertainty[6, 11].

In order to overcome these difficulties and uncertainties, the delayed field ionization technique was adopted in this paper to detect the bound Rydberg state of Sm atoms according to the relationship between the first ionization threshold of Sm atoms and the varying electric field. By controlling the delay time between the electrostatic field and the pulsed ionizing electric field, the ions generated by photoionization[23-24] and autoionization are pushed out of the action zone before the application of pulsed electric field and only the Sm atoms in the bound Rydberg state are detected. Thus the first ionization threshold under the electric field can be clearly observed. The first ionization thresholds of Sm atoms under different electrostatic field intensities were fitted to obtain the first ionization threshold under zero field. Then the reliability of this method was verified by comparison with the value in the literature[6, 21]. The effect of different magnetic quantum numbers on the first ionization threshold of Sm atom was also studied by using different polarization combinations for excitation.

2　Experimental setup and principle

2.1　Experimental setup

The experimental facilities in this paper include: laser system, atomic beam preparation system, and signal acquisition and analysis system, as shown in Fig. 1. The laser system consists of one Nd:YAG solid state laser (GNT 0021-0805/L) and three tunable dye lasers manufactured by Quanta System. The laser light output by the solid-state laser has a pulse width of 6~8 ns, a frequency of 20 Hz, and a fundamental frequency wavelength of 1 064 nm. After the frequency doubling, 532 nm pulse laser is output to pump the three dye lasers. By tuning, the three dye lasers output the 672.773 nm, 654.255 nm and 650.000~653.500 nm laser light respectively, whose linewidth is 0.1 cm^{-1}. The three-step laser λ_1, λ_2 and λ_3 passes through a polarizing plate and a half-wave or quarter-wave plate respectively to ensure the desired polarization state for the experiment. Because the energy level density of Sm atoms is very high, the three-step laser enters the vacuum chamber successively with a delay of 8 ns to ensure that the Sm atoms are excited to the selected Rydberg state in succession and to avoid unnecessary excitation.

In Fig. 1, the parts within the dotted circle, including atomic beam generator, laser-atom interaction area and ion detector (microchannel plate), are in a vacuum environment. The pressure in the vacuum chamber can be maintained below 2.0×10^{-5} Pa by a combination of mechanical pump and molecular pump. By use of tantalum heating wire and temperature control device, the temperature of atomic furnace is kept at 837 K. The generated Sm atom vapor is ejected from the hole of atomic furnace. In order to avoid the Doppler broadening effect of spectral line, the ejected Sm atom beam should be orthogonal to the laser beam after collimation. The electric field in the area where the laser interacts with Sm atoms is obtained by applying voltage on two parallel metal plates with a distance of 1 cm. The grid in the middle of each metal plate ensures that the electric field in the action zone is uniform and that the ionized Sm^+ ions can fly out of the action zone. After using a 2280S-60-3 DC power supply manufactured by Keithley to apply DC voltage to the polar plate near the microchannel plate, an electric field is formed with an intensity of no more than 60 $V\cdot cm^{-1}$ (accuracy: $\pm10^{-4}$ $V\cdot cm^{-1}$). At the first and second excitation steps, the principal quantum number of Sm atoms in the intermediate state excited by laser is $n\leqslant7$, and the Stark effect can be ignored. At the final excitation step, the principal quantum number in the Rydberg state excited

by laser is larger, the Stark effect is significant, and the Sm atoms whose energy is higher than the first ionization threshold of electric field are ionized. In addition to the excitation of Sm atoms to a predetermined Rydberg state, Sm^+ ions may be generated by the photoionization process (such as $\lambda_1+2\lambda_3$ excitation) and the autoionization process resulting from Rydberg atom collisions. The Sm^+ ions generated by these processes will be superposed on the Rydberg state spectrum to cause interference, making the spectral signal-to-noise ratio worse and the first ionization threshold impossible to be directly observed. After connecting the polar plate far from the microchannel plate to a AVRH-3-B-PN pulsed power supply made by Avtech, an electric field is formed with an amplitude of 3000 $V\cdot cm^{-1}$ (accuracy: ±1 $V\cdot cm^{-1}$). Pulsed electric field is used to ionize the Sm atoms in Rydberg state below the ionization threshold in the electrostatic field and collect the generated Sm^+ ions. To prevent the Sm^+ ions generated by other processes from interfering with the spectrum measurement and improve the measurement precision, a 9650 pulse delay generator made by AMETEK can be used to control the delay time between pulsed electric field and the laser λ_3 so as to ensure that the Sm^+ ions generated by other processes will fly out of the action zone from the polar plate far away from the microchannel plate before the action of pulsed electric field without being detected.

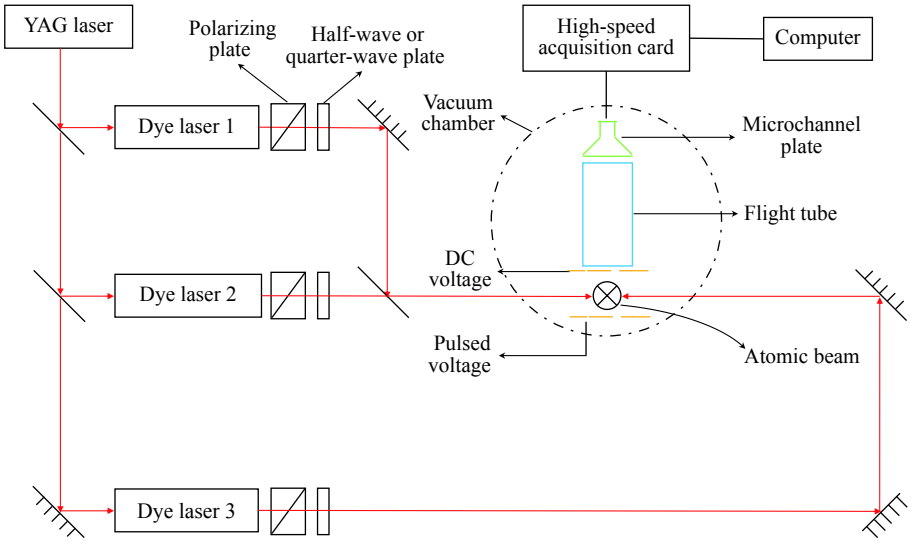

Fig. 1 Experimental setup diagram

图 1 实验装置图

The Sm^+ ions out of the polar plate near a microchannel plate will fly freely through a flight-path tube to the high-gain (about 10^8), fast-response microchannel plate, where a large number of electrons will be produced. A high-speed acquisition card (model: U1071A) made by Agilent Technologies is used to convert the analog signal amplified by microchannel plate into a digital signal and then output it to a computer for further analysis and processing.

The energy in the spectrogram is determined by the sum of the energy of $4f^6 6s7s\ ^7F_2$ state[25] and the photon energy of λ_3. For the three dye lasers, the laser linewidth generated by them is 0.1 cm^{-1}, and the laser wavelength can be measured with the WaveMaster wavelength meter made by Coherent Inc. with the accuracy up to 0.01 cm^{-1}. The laser beam is perpendicular to the atomic beam, thus min-

imizing the spectral broadening effect caused by the Doppler effect. In addition, we measured the same spectrum for several times to minimize the random error in wavelength. Therefore, the energy uncertainty obtained in this experiment is ±0.1 cm^{-1}, which is mainly determined by the laser linewidth.

2.2 Experimental principle

The spectral measurement includes the measurement of absorption spectrum[26] and emission spectrum[27]. In this paper, Sm atoms are successively excited to the $4f^6 6snp$ Rydberg series near the first ionization threshold along the path shown in Fig. 2 by use of absorption spectrum and three-color three-photon method. Because the maximum energy difference between the ground state of Sm atom ($4f^6 6s^2\ ^7F_0$) and the six metastable states above it ($4f^6 6s^2\ ^7F_J$(J = 1-6)) is only 4 020.66 cm^{-1}[25], the ground state and the six metastable states all have an atom population due to thermal population. In order to excite the Sm atoms to the maximum scale and to simplify the total angular momentum and magnetic quantum number of the Rydberg state, we choose the ground state $^7F_0$ as initial energy level. At first, the laser at the wavelength λ_1 =672.773 nm excites, through resonance, one of the 6s electron in the Sm atom of $4f^6 6s^2\ ^7F_0$ state to 6p state, where the Sm atom is in the intermediate state $4f^6 6s6p\ ^9F_1$. Then the laser at the wavelength λ_2=654.255 nm further excites the valence electron to 7s state, where the Sm atom is in the $4f^6 6s7s\ ^7F_2$ state. Finally, the laser at λ_3 scans the 650.000~653.500 nm range, exciting the Sm atom in electric field to a bound or autoionizing Rydberg state with the energy range covering the first ionization threshold. In the electric field, the first ionization threshold will be lowered, the Sm atoms in Rydberg state above the first ionization threshold will be ionized, and the generated ions will fly out of the polar plate far away from the microchannel plate without being detected. By applying a pulsed electric field with an amplitude of 3 000 $V \cdot cm^{-1}$, the Sm atoms in Rydberg state below the first ionization threshold will be ionized, and the generated ions will fly out of the polar plate close to the microchannel plate and get detected. Since the laser pulse width is 6~8 ns, the optical path should be changed to control the time for the above three-step laser to reach the action zone with a delay of 8 ns between steps so as to ensure that the Sm atom could absorb the photons λ_1, λ_2 and λ_3 one by one, as shown in Fig. 2. The energy level structure of Sm atoms is very complex, so two of the above laser beams may also cause the photoionization of Sm atoms, for example $\lambda_1+2\lambda_3$. To avoid the influence of these interference peaks, we kept λ_1 or λ_2 off and then scanned λ_3 to identify it, thus ensuring that the data used in the analysis was the result of three-step light effect.

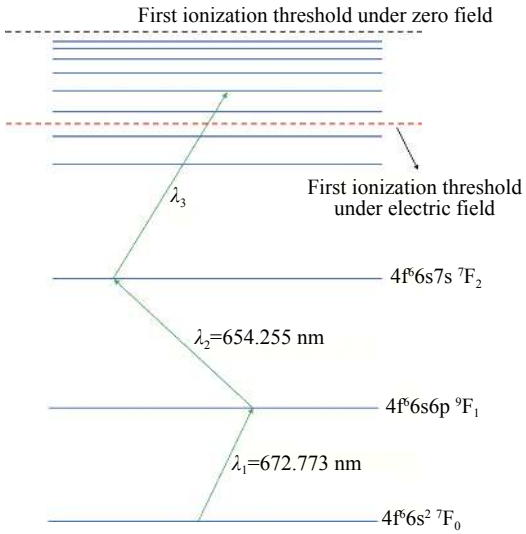

Fig. 2　Schematic diagram of multistep excitation path of Sm atom

图 2　Sm 原子的多步激发路径示意图

In this paper, the atoms in Rydberg state below the first ionization threshold are detected by the delayed-field ionization technique. In addition to this process, the following processes can also generate the Sm^+ ions: (1) if the energy of Sm atoms in Rydberg state is higher than the first ionization threshold under the electric field, then the electrostatic field ionization of Sm atoms will generate the Sm^+ ions; (2) when a Sm atom absorbs the λ_1 and λ_2

photons to enter the $4f^6 6s7s\ ^7F_2$ state and the energy of the λ_3 photon is greater than the ionization energy of $4f^6 6s7s\ ^7F_2$ state, the Sm atom in $4f^6 6s7s\ ^7F_2$ state will have a certain chance to be stimulated into the continuous state $4f^6 6s\varepsilon p$ and then ionized (direct non-resonance photoionization); (3) due to the complexity of energy level structure of Sm atoms, the photoionization processes such as $\lambda_1+2\lambda_3$ and $\lambda_1+\lambda_2+2\lambda_2$ will also generate the Sm^+ ions; (4) the collisions between the atoms in highly excited Rydberg state converging to the first ionization threshold can generate the Sm^+ ions, but a very wide autoionization peak near the threshold makes it difficult to directly observe the position of the threshold; (5) through resonance, the λ_3 photon excites the Sm atom in $4f^6 6s7s\ ^7F_2$ state into the autoionizing state to generate the Sm^+ ions. It should be noted that in both the processes (2) and (5), the Sm atom in $4f^6 6s7s\ ^7F_2$ state absorbs a λ_3 photon and then is ionized. However, the process (2) is a direct photoionization process realized by exciting the $4f^6 6s7s\ ^7F_2$ state into the continuous state $4f^6 6s\varepsilon p$, and belongs to non-resonance ionization with a small ionization cross section. The process (5) is a autoionization process exciting the $4f^6 6s7s\ ^7F_2$ state into a autoionization state (such as $4f^6 5d7s$) to generate the Sm^+ ions, and belongs to resonance ionization with a large ionization cross section. In the above processes, the Sm^+ ions are generated before the action of delayed pulsed electric field. By applying an electrostatic field that reverses the pulsed electric field and ensuring that the delay time between pulsed electric field and λ_3 is long enough, the Sm^+ ions can fly out of the action zone from the electric field polar plate far from the microchannel plate. Even if not all of these Sm^+ ions fly away from the polar plate far from the microchannel plate, they will be completely separated in time from the Sm^+ ions produced by the ionization of bound Rydberg state. In this way, all the obtained spectral signals are generated by the Sm atoms in bound Rydberg state under the electric field, so the spectral signal-to-noise ratio can be greatly improved, and the position of the first ionization threshold under the electric field can also be directly observed. The experimental law under which the position of the first ionization threshold varies with the electric field intensity can be obtained by changing the electrostatic field intensity. According to Rydberg-Ritz formula[25]:

$$n^* = \sqrt{\frac{R_{Sm}}{I_0 - E_{Ryd}}} \quad , \qquad (1)$$

where R_{Sm} = 109 736.92 cm^{-1} is the Rydberg constant of Sm atom, E_{Ryd} is the energy of Sm atom in Rydberg state, I_0 is the first ionization threshold of Sm atom under zero field, n^* is the effective quantum number of Sm atom in Rydberg state.

According to the threshold ionization field of Sm atom in Rydberg state [28]:

$$F = \frac{1}{16n^{*4}} \quad , \qquad (2)$$

where F is the intensity of electric field in atomic unit.

Thus, the relationship between the first ionization threshold I of Sm atom under the electric field and the electric field intensity F is

$$I = I_0 - 4R_{Sm}\sqrt{F} \quad . \qquad (3)$$

According to Eq. (3), the first ionization threshold I_0 of Sm atom under zero field can be fitted from the experimental data.

In a multistep resonant transition, the total probability of the transition from ground state to highly excited state depends on the polarization state of the light at each step and on all the atomic states involved in the transition. In an electric dipole transition, the transition probability W_1 is proportional to the square of the Wigner 3J symbol modal associated with the transition[29]:

$$W_1 \propto \begin{bmatrix} J_2 & 1 & J_1 \\ -M_2 & \varphi & M_1 \end{bmatrix}^2 \quad , \qquad (4)$$

where J_1 and M_1 are the total angular momentum quantum number and magnetic quantum number of initial transition state; J_2 and M_2 are the total angular momentum quantum number and magnetic quantum number of final transition state; φ is the magnetic quantum number of photon, φ= 0 when the laser is linearly polarized (π), and φ= ±1 when it is circularly polarized (σ±). For the transition with two or more steps, the total transition probability W is equal to the product of the transition probabilities at all the steps. It should be noted that, for the vertical linear polarized light (πσ combination), the polarized light at the second step needs to be decomposed into right-handed and left-handed circular polarized light (σ^+ and σ^-) due to the difference in the quantization axes of the two steps. In this case, φ_1= 0, φ_2= ±1. Under zero field, the degeneracy of energy level is 2J+1 for the atomic state with the total angular momentum quantum number of J, and the value range of magnetic quantum number M is −J~J. So the total transition probability is

$$W \propto \sum_{q} \prod_{i=1}^{k} \left| \begin{bmatrix} J_i & 1 & J_{i-1} \\ -M_i & \varphi_i & M_{i-1} \end{bmatrix} \right|^2, \qquad (5)$$

where k is the number of steps in the transition, and q is the number of possible transitions after considering the degeneracy of all the energy levels involved in the transition. According to the excitation path 0→1→2→1−3 of the total angular momentum quantum number proposed in this paper, the value range of the magnetic quantum number in final state is −3~3. Take the polarization combination ππσ as an example. According to Eq. (5), the transition is probable only in the final states with the magnetic quantum numbers of ±1, while the transition probability in the final states with other magnetic quantum numbers is 0. The magnetic quantum numbers of final states obtained by other polarization combinations are shown in Table 1. By using the three polarization combinations in Table 1, the relationship between the first ionization threshold (I_0) of Sm atom and the magnetic quantum number (m) in final state was also explored in this paper.

Tab. 1　Magnetic quantum numbers of Sm atom in $4f^6 6sn\mathit{k}$ state excited by different polarization combinations of λ_1, λ_2 and λ_3

表 1　λ_1,λ_2 和 λ_3 不同偏振态组合激发下 $4f^6 6sn\mathit{k}$ 态 Sm 原子的磁量子数

Combination 组合	Polarization state 偏振状态			Magnetic quantum number 磁量子数
	λ_1	λ_2	λ_3	m
1	π	π	π	0
2	π	π	σ	±1
3	σ^+	σ^+	σ^+	3

3　Results and discussion

When the delay time t_d between pulsed electric field and λ_3 is 0.3 μs and 35.8 μs, the spectra of Sm atoms near the first ionization threshold under zero and electric fields are obtained, as shown in Fig. 3. The dotted line shows the position of the first ionization threshold I_0=45 519 cm^{-1} under zero field[25]. The symbol "*" represents the autoionization state above the first ionization threshold. What's in the dashed box is the autoionization state with a large linewidth caused by Rydberg atom collision effect. As shown in Fig.3(a), the Rydberg energy level below the first ionization threshold obviously converges to the threshold under zero field at t_d = 0.3 μs. At the same time, a wide autoionization peak (dashed box) appears near the first ionization threshold, so that the threshold cannot be clearly seen; and a very strong resonance autoionization peak ("*") is observed above the threshold. As shown in Fig. 3(b), the Rydberg atom signal far from the first ionization threshold disappears when the delay time increases to 35.8 μs. This is because the Rydberg state near the first ionization threshold has a lower principal quantum number and a shorter lifetime than the Rydberg State far from the threshold. As a

result, when the pulsed electric field is active, these Rydberg atoms with lower principal quantum numbers have already jumped to lower energy levels and can't be detected. This also implies that the delay time cannot last too long when the Rydberg state of Sm atom is studied through delayed field ionization. The comparison of Fig. 3(a) and Fig. 3(c) shows that, when the delay time is relatively short, the autoionization signal under the 0.500 0 V·cm^{-1} electrostatic field remains basically unchanged compared with that under zero field. This means that the electrostatic field fails to push the autoionized ions out of the action zone within such a short delay, and thus the autoionization signal and the Rydberg signal overlap so that the position of the first ionization threshold cannot be directly observed in the spectrum. In the Fig. 3(d), the delay time of pulsed electric field increases to 35.8 μs with the presence of 0.499 5 V·cm^{-1} electrostatic field. Because the delay time is long enough, the autoionization ions have been pushed out of the action zone by electrostatic field without being detected when the pulsed electric field is applied. In the spectrogram, the very strong resonant autoionization signal completely disappears so that the first ionization threshold under the electrostatic field can be directly observed.

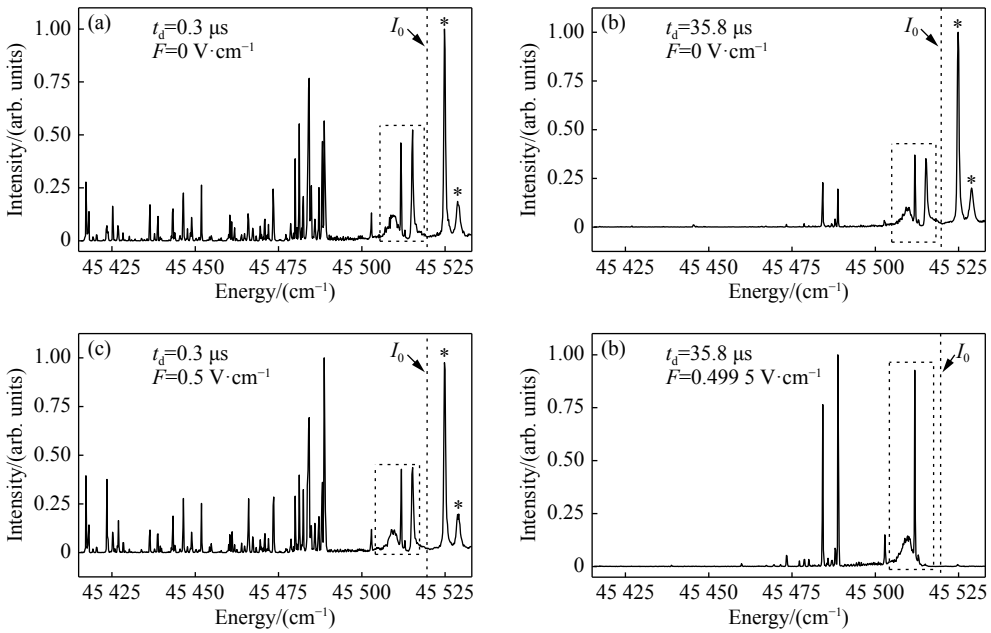

Fig. 3 Spectra of the Sm atom near the first ionization threshold under zero and electric fields

图 3 零场和电场下 Sm 原子在第一电离阈附近的光谱图

As shown in Fig. 4, when the amplitude of pulsed electric field was 3 000 V·cm^{-1} and the t_d was 35.8 μs, the spectra of Sm atoms around the first ionization threshold under zero field and the electrostatic fields with different intensities were obtained. The symbol "*" indicates a resonant autoionization state that is very strong above the first ionization threshold. It can be seen that, as the interference of autoionization and photoionization signals and other signals is eliminated under the electrostatic field, the spectral signal-to-noise ratio has been significantly improved and the first ionization threshold can be observed very clearly. With the increase of electric field intensity, the wider autoionization envelope below the first ionization threshold gradually disappears and the threshold moves to a significantly lower energy level according to the movement law described by Eq. (3).

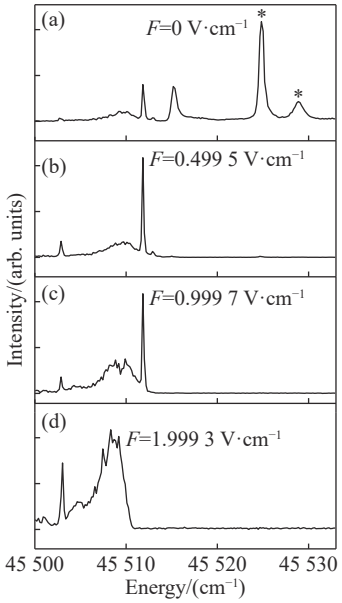

Fig. 4　Spectra of the Sm atom near the first ionization threshold under zero and electric fields at t_d=38.5 μs

图 4　t_d=38.5 μs 时, 在零场和电场下 Sm 原子第一电离阈附近的光谱图

When t_d was 35.8 μs and an electrostatic field was applied, only the field ionization signal of Sm atoms in Rydberg state below the first ionization threshold was detected. Therefore, the position near the first ionization threshold where the signal suddenly increased was selected as the position of the first ionization threshold of Sm atoms under the electrostatic field. The position indicated by an arrow in Fig. 5 is just the position of the first ionization threshold of Sm atoms under the 1.999 3 V·cm^{-1} electrostatic field.

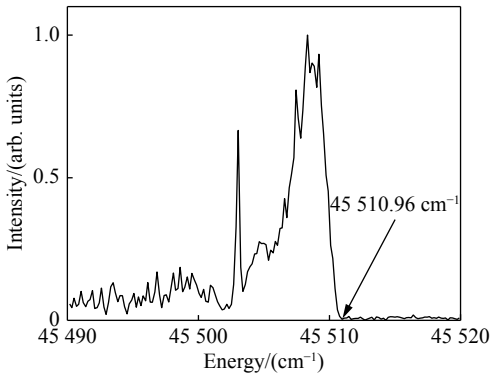

Fig. 5　Spectra of Sm atom under the electrostatic field of 1.999 3 V·cm^{-1}

图 5　Sm 原子在静电场为 1.999 3 V·cm^{-1} 时的光谱图

Thus, by changing the electrostatic field intensity, the position of the first ionization threshold of Sm atoms under different electrostatic fields can be obtained, as shown in Fig. 6. The circle in the figure represents the experimental data, and the solid line represents the curve fitted according to Eq. (3). The polarization combinations of the three-step lasers λ_1, λ_2 and λ_3, as shown in Fig. 6(a), Fig. 6(b) and Fig. 6(c), correspond to the combinations 1, 2 and 3 in Table 1 respectively.

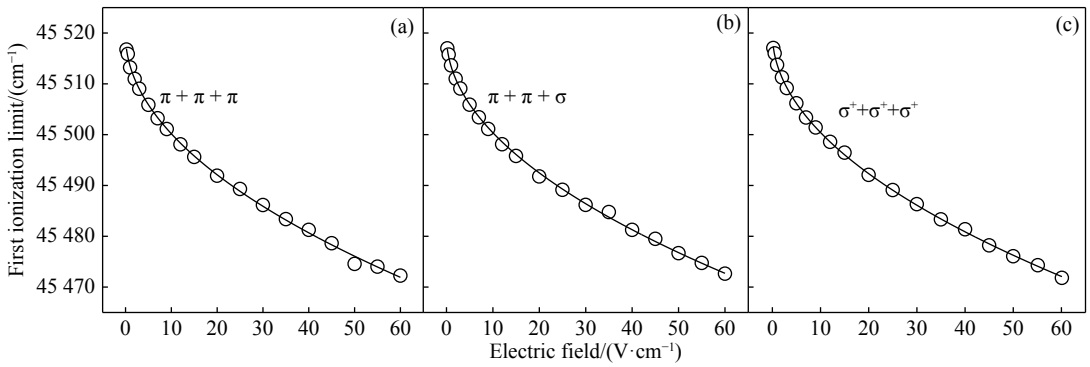

Fig. 6　Diagram of the first ionization threshold of Sm atom shifting with the change of electrostatic field intensity under different polarization combinations of three-step lasers. (a) π + π+ π; (b) π + π+ σ; (c) $\sigma^+ + \sigma^+ + \sigma^+$

图 6　三步激光不同偏振组合下, Sm 原子第一电离阈随静电场强度改变而移动的规律图。(a) π + π+ π; (b) π + π+ σ; (c) $\sigma^+ + \sigma^+ + \sigma^+$

The Table 2 lists the fitting results of the first ionization thresholds of Sm atoms in Rydberg state with different magnetic quantum numbers under zero field. According to the fitting results, the maximum difference of the first ionization thresholds under zero field is only 0.49 cm^{-1}. The average value of the three combinations, namely I_0 = 45519.69±0.17 cm^{-1}, is the first ionization threshold of Sm atoms under zero field, and is in good agreement with the reference value 45519.64±1.39 cm^{-1}[6]. This demonstrates the effectiveness of using the law of ionization threshold shift in electric field to obtain the ionization threshold under zero field.

Tab. 2 Fitting results of the first ionization threshold of the Sm atom with different magnetic quantum numbers

表 2 不同磁量子数的 Sm 原子零场下第一电离阈的拟合结果

Combination 组合	Magnetic quantum number, m 磁量子数m	Ionization threshold/ cm^{-1} 电离阈/ cm^{-1}
1	0	45519.67±0.21
2	±1	45519.46±0.18
3	3	45519.95±0.11

4 Conclusion

In this paper, a pulsed electric field was used to detect the delayed field ionization of Sm atoms in highly excited Rydberg state. By applying a reverse electrostatic field before the generation of pulsed electric field and increasing the delay time, the ion signal interference caused by photoionization, autoionization and other paths was eliminated and the signal-to-noise ratio in the experiment was improved. By changing the intensity of electrostatic field, the shift of the first ionization threshold of Sm atoms was observed and studied. Meanwhile, by changing the polarization combination of the three-step laser, the position of the first ionization threshold of Sm atom with different magnetic quantum numbers under zero field was precisely determined. The first ionization threshold of Sm atom finally obtained was 45519.69±0.17 cm^{-1}, which was consistent with the reference values determined by other methods, thus demonstrating the reliability of the proposed method.

——中文对照版——

1 引 言

第一电离阈是决定元素化学性质最重要的原子特性参数之一[1-2]。第一电离阈的精确测量对理解元素的电子结构和化学特性都非常有帮助[3]。对于重元素而言，不仅需要考虑库仑相互作用，还需要考虑电子-电子关联、量子电动力学和相对论效应，这使得精确测量重元素的第一电离阈非常困难[1, 3-5]。通常测量第一电离阈的方法有：共振电离质谱法[1]、Rydberg 能级收敛法[6-7]、表面电离技术[8] 和电场电离阈移动法[9] 等。

对于镧系稀土原子这类重元素而言，大多具有未填满的 4f 次壳层，其高激发态因可能同时包含最外层电子和 4f 次壳层电子的跃迁，导致其光谱非常复杂[5, 10-15]。尤其对于 Sm 原子而言，由于 Sm 原子基态 $4f^6 6s^2\ ^7F_0$ 上方存在着 $4f^6 6s^2\ ^7F_J$(J 为 1~6) 这 6 个亚稳态，当加热 Sm 金属制备原子样品时，这些亚稳态上也会有布居，这导致 Sm 原子的跃迁初态有多种可能，并且 Sm 原子具有 8 个价电子，这一特点使得在同一电子组态下会存在非常多的原子状态，所以 Sm 原子的能级结构极其复杂。总之，Sm 原子的这些特点会导致其原子光谱相比于其它稀土原子而言更具有挑战性[16-19]。类似于稀土 Yb 原子[20]、Ho 原子[21]、Eu 原子[9] 和碱土 Ba 原子[22]，由于收敛于第一电离阈的高激

发 Rydberg 态原子间碰撞几率增加, Sm 原子在第一电离阈附近也存在很宽的自电离峰, 导致很难直接观察到第一电离阈的位置, 通常需要 Rydberg-Ritz 公式对 Rydberg 系列的能级数据进行拟合才能得到[6-7, 21]。然而, 由于多步激发以及原子能级的复杂性, 在高激发态光谱中, 除了 Rydberg 系列以外, 通常会出现一些非 Rydberg 系列的干扰能级, 使得不确定性增加[6, 11]。

为了克服这些困难与不确定性, 考虑 Sm 原子第一电离阈随电场移动的关系, 本文采取延时场电离探测技术来探测束缚 Rydberg 态 Sm 原子。通过控制静电场和脉冲电离电场的延时时间, 保证光电离[23-24] 和自电离过程产生的离子在施加脉冲电场之前被推出作用区而只探测束缚 Rydberg 态 Sm 原子。这样就可以清楚地观察到电场下的第一电离阈。通过不同静电场强度下的 Sm 原子第一电离阈拟合得到零场下 Sm 原子的第一电离阈, 并与文献值 [6, 21] 比较验证该方法的可靠性。同时通过不同的偏振组合激发, 研究了不同磁量子数对 Sm 原子第一电离阈的影响。

2　实验装置与原理

2.1　实验装置

本文实验装置包括以下几个部分: 激光系统、原子束制备系统和信号采集与分析系统, 如图 1 所示。激光系统是由 Quanta System 公司生产的一台 Nd: YAG 固体激光器(型号为 GNT 0021-0805/L)和 3 台可调谐的染料激光器组成。该固体激光器输出激光的脉冲宽度为 6~8 ns, 频率为 20 Hz, 基频光波长为 1 064 nm, 经过倍频后输出 532 nm 的脉冲激光, 用于泵浦 3 台染料激光器。通过调谐, 3 台染料激光器分别输出 672.773 nm、654.255 nm 和 650.000~653.500 nm 的激光, 其线宽为 0.1 cm^{-1}。三步激光 λ_1, λ_2 和 λ_3 分别通过偏振片和半波片或四分之一波片, 确保达到实验所需的偏振状态。因为 Sm 原子的能级密度非常高, 三步激光依次延时 8 ns 进入真空腔, 保证 Sm 原子依次激发至选择的 Rydberg 态而避免不必要的激发。

在图 1 中虚线圆的部分都是处于真空环境, 包括原子束产生装置、激光与原子相互作用区、离子探测装置(微通道板)。利用机械泵 - 分子泵的组合, 真空腔里的压强可以维持在 2.0×10^{-5} Pa 以下。通过钽加热丝和温控装置保证原子炉温度在 837 K, 产生的 Sm 原子蒸气从原子炉的小孔喷出。为了尽量避免谱线的 Doppler 展宽效应, 喷出的 Sm 原子束经过准直后与激光束正交。激光与 Sm 原子作用区的电场通过在两个距离为 1 cm 的平行金属板上施加电压实现, 每个金属板中间的栅网既保证了作用区的电场为均匀电场又保证了电离后的 Sm^+离子可以飞出作用区。在靠近微通道板的电场极板上通过 Keithley 公司生产的型号为 2280S-60-3 的直流电源施加直流电压, 产生的电场强度不大于 60 $V\cdot cm^{-1}$, 精度为$\pm10^{-4}$ $V\cdot cm^{-1}$。第一、二步激光所激发的 Sm 原子中间态主量子数 $n\leqslant7$, Stark 效应可以忽略, 最后一步光激发的 Rydberg 态主量子数较大, 此时会产生明显的 Stark 效应, 并且能量高于电场下第一电离阈的 Sm 原子会被电离。除了 Sm 原子会被激发到预定的 Rydberg 态之外, 由于 Sm 原子能级的复杂性, 可能还会存在 $\lambda_1+2\lambda_3$ 激发等光电离过程和 Rydberg 原子碰撞导致的自电离过程产生的 Sm^+离子。以上这些过程产生的 Sm^+离子会叠加在 Rydberg 态光谱上从而产生干扰, 使得光谱信噪比变差以及第一电离阈无法直接观察到。在远离微通道板的电场极板上接入 Avtech 公司生产的型号为 AVRH-3-B-PN 的脉冲电源, 产生的脉冲电场幅值为 3 000 $V\cdot cm^{-1}$, 精度为±1 $V\cdot cm^{-1}$。脉冲电场的作用为电离在静电场中低于电离阈的 Rydberg 态 Sm 原子并收集产生的 Sm^+离子。为了不让其它过程产生的 Sm^+离子干扰光谱测量, 提高测量精度, 可以通过 AMETEK 公司 9 650 型脉冲延时发生器控制脉冲电场与激光 λ_3 之间的延时, 保证其它过程产生的 Sm^+离子在脉冲电场作用前从远离微通道板的电场极板飞出作用区而不被探测到。

从接近微通道板的电场极板飞出的 Sm^+离子通过飞行管道自由飞行至高增益(增益约为 10^8)、快响应的微通道板上产生大量的电子。利用 Agi-

lent Technologies 公司生产的高速采集卡(型号 U1071A)对经过微通道板放大的信号进行模拟 - 数字转换后输入计算机,以进行进一步的分析和处理。

光谱图中的能量由参考文献 [25] 中的 $4f^6 6s7s\ ^7F_2$ 态的能量与 λ_3 的光子能量之和确定。3 台染料激光器产生的激光线宽为 0.1 cm^{-1},其中激光波长使用相干公司的 WaveMaster 波长计测量得到,精度可以达到 0.01 cm^{-1}。激光和原子束的方向垂直,这样最大程度地避免了多普勒效应导致的光谱加宽。另外,也对同一光谱进行了多次测量,以便把波长的随机误差减到最小。所以,本实验获得的能量不确定度为±0.1 cm^{-1},这主要是由激光线宽决定的。

2.2 实验原理

光谱测量包括吸收光谱[26] 和发射光谱[27] 两种,本文使用吸收光谱,采用三色三光子将 Sm 原子依次激发至第一电离阈附近的 $4f^6 6snp$ Rydberg 系列。激发路径如图 2 所示。因为 Sm 原子基态 $4f^6 6s^2\ ^7F_0$ 与其上方的 6 个亚稳态 $4f^6 6s^2\ ^7F_J(J=1-6)$ 的最大能量差仅为 4020.66 cm^{-1}[25],由于热布居使得基态和这 6 个亚稳态均有原子布居。为了最大比例地激发 Sm 原子和使 Rydberg 态的总角动量和磁量子数简单,本文选择基态 $^7F_0$ 作为初始能级。首先,波长为 λ_1 =672.773 nm 的激光将处于 $4f^6 6s^2\ ^7F_0$ 态的 Sm 原子其中一个 6s 态电子共振激发到 6p 态,此时 Sm 原子处于 $4f^6 6s6p\ ^9F_1$ 中间态。然后,波长为 λ_2=654.255 nm 的激光进一步激发该价电子到 7s 态,此时 Sm 原子处于 $4f^6 6s7s\ ^7F_2$ 态。最后,λ_3 在 650.000~653.500 nm 范围内扫描,在电场中将 Sm 原子激发到束缚或自电离 Rydberg 态,能量范围覆盖第一电离阈。在电场下第一电离阈会降低,高于第一电离阈的 Rydberg 态将会被电离,产生的离子会从远离微通道板的极板飞出而不会被探测到。通过施加幅值为 3000 $V\cdot cm^{-1}$ 的脉冲电场,使得低于第一电离阈的 Rydberg 态 Sm 原子被电离,产生的离子会从靠近微通道板的极板飞出而被探测到。因为激光脉宽为 6~8 ns,为确保 Sm 原子按照图 2 所示依次吸收 λ_1, λ_2 和 λ_3 光子,需要通过改变光程来控制上述 3 步激光到达作用区的时间,使其依次延时 8 ns。由于 Sm 原子能级结构非常复杂,因此,上述激光中的两束激光也可能使 Sm 原子光电离,如 $\lambda_1+2\lambda_3$。在本文中,为了避免这些干扰峰的影响,通过挡住 λ_1 或 λ_2 再扫描 λ_3 将其识别出来,以确保数据分析时所用的数据都是三步光作用的结果。

本文采用延时场电离技术来探测第一电离阈以下的 Rydberg 态原子,除了该过程中产生的 Sm^+离子,还会存在以下过程产生的 Sm^+离子:(1)Rydberg 态 Sm 原子如果能量高于电场下的第一电离阈,那么通过静电场场电离会产生 Sm^+离子;(2) Sm 原子依次吸收 λ_1 和 λ_2 光子处于 $4f^6 6s7s\ ^7F_2$ 态时,只要 λ_3 光子的能量大于 $4f^6 6s7s\ ^7F_2$ 态的电离能,处于 $4f^6 6s7s\ ^7F_2$ 态的 Sm 原子就有一定几率被激发至连续态 $4f^6 6s\varepsilon p$ 而电离,这种电离方式为直接光电离,属于非共振电离;(3) 由于 Sm 原子能级结构的复杂性,还会存在 $\lambda_1+2\lambda_3$、$\lambda_1+\lambda_2+2\lambda_2$ 等光电离过程产生的离子;(4) 由于收敛于第一电离阈的高激发 Rydberg 态原子间碰撞产生的离子,在第一电离阈附近存在很宽的自电离峰,导致很难直接观察到第一电离阈的位置;(5) 存在 λ_3 光子将处于 $4f^6 6s7s\ ^7F_2$ 态的 Sm 原子共振激发至自电离态,通过自电离过程产生的离子。需要注意的是,过程 (2) 和 (5) 都是处于 $4f^6 6s7s\ ^7F_2$ 态的 Sm 原子吸收一个 λ_3 光子而电离。过程 (2) 是直接光电离过程,由 $4f^6 6s7s\ ^7F_2$ 态激发至连续态 $4f^6 6s\varepsilon p$ 而电离,属于非共振电离,电离截面较小;而过程 (5) 是自电离过程,由 $4f^6 6s7s\ ^7F_2$ 态激发至自电离态,如 $4f^6 5d7s$,进一步通过自电离过程产生 Sm^+离子,属于共振电离,电离截面较大。在上述过程中产生的 Sm^+离子都是在延时脉冲电场作用之前产生的。通过施加与脉冲电场反向的静电场,并保证脉冲电场与 λ_3 之间的延时时间足够长,使得这些 Sm^+离子从远离微通道板的电场极板飞出作用区,或者即使没有完全从远离微通道板的电场极板飞出,这些 Sm^+离子也会与束缚 Rydberg 态电离产生的 Sm^+离子在时间上完全分开。这样获得的光谱信号则全部是由电场下束缚 Rydberg 态 Sm 原子产生,使得光谱信噪比大大提高,并且也能直接观测到电场下第一电离阈的位置。通过改变静电场强度可以得到第一电离阈的位置随电场强度变化的实验规律。根据 Ry-

dberg-Ritz 公式[25]:

$$n^* = \sqrt{\frac{R_{\mathrm{Sm}}}{I_0 - E_{\mathrm{Ryd}}}} \quad , \qquad (1)$$

其中, R_{Sm}=109 736.92 cm^{-1} 是 Sm 原子 Rydberg 常数, E_{Ryd} 是 Rydberg 态 Sm 原子的能量, I_0 是零场下的 Sm 原子的第一电离阈, n^*为 Rydberg 态 Sm 原子的有效量子数。Rydberg 态 Sm 原子的阈值电离电场为: [28]

$$F = \frac{1}{16n^{*4}} \quad , \qquad (2)$$

其中, F 为原子单位下的电场强度。由此, 可以得到电场下 Sm 原子第一电离阈 I 与电场强度大小 F 的关系:

$$I = I_0 - 4R_{Sm}\sqrt{F} \quad . \qquad (3)$$

根据公式(3), 由实验数据可以拟合出零场下的 Sm 原子的第一电离阈 I_0。

在多步共振跃迁中, 从基态到高激发态的总的跃迁几率取决于每步光的偏振状态和所有参与跃迁的原子态。在电偶极跃迁中, 跃迁几率 W_1 正比于与跃迁有关的 Wigner 3J 符号模的平方[29]:

$$W_1 \propto \begin{bmatrix} J_2 & 1 & J_1 \\ -M_2 & \varphi & M_1 \end{bmatrix}^2 \quad , \qquad (4)$$

其中 J_1、M_1 为跃迁初态的总角动量量子数和磁量子数, J_2、M_2 为跃迁末态的总角动量量子数和磁量子数, φ 表示光子的磁量子数, 激光为线偏振光 (π) 时, φ=0, 为圆偏振 (σ$^{\pm}$) 时 φ 取±1。对于两步及以上跃迁, 总的跃迁几率 W 等于每步跃迁几率之积。需要注意的是, 对于垂直线偏振光 (πσ 组合), 由于两步光量子化轴不同, 需要将第二步线偏振光分解为右旋和左旋圆偏振光两部分 (σ$^+$和 σ$^-$), 此时 φ_1 取 0 而 φ_2 取±1。在零场下, 对于总角动量量子数为 J 的原子态而言能级简并度为 2J+1,磁量子数 M 的取值范围为−J~J。所以总的跃迁几率为:

$$W \propto \sum_q \prod_{i=1}^{k} \left\| \begin{bmatrix} J_i & 1 & J_{i-1} \\ -M_i & \varphi_i & M_{i-1} \end{bmatrix} \right\|^2 \quad , \qquad (5)$$

其中 k 表示跃迁的步数, q 表示考虑所有参与跃迁的能级的简并度以后可能跃迁的数目, 如文中所采用的总角动量量子数 0→1→2→1−3 的激发路径, 终态磁量子数的取值范围为−3~3。以偏振组合 ππσ 为例, 根据公式(5)只有磁量子数为±1 的终态才会存在跃迁的可能, 而其它磁量子数的终态跃迁几率为零。通过其它偏振组合获得的终态的磁量子数如表 1 所示。通过表 1 中的 3 种偏振组合, 本文同时探索了 Sm 原子的第一电离阈 I_0 与终态磁量子数 m 之间的关系。

3　结果与讨论

当脉冲电场与 λ_3 之间的延时 t_{d} 分别为 0.3 μs 和 35.8 μs 时, 得到了零场和电场下 Sm 原子在第一电离阈附近的光谱图, 如图 3 所示。虚线表示文献 [25] 中零场下的第一电离阈 I_0=45 519 cm^{-1} 的位置, "*"号表示第一电离阈以上的自电离态, 虚线框内是由于 Rydberg 原子碰撞效应导致的较宽线宽的自电离态。从图 3(a) 可以看到, 在零场下, 当 t_{d}=0.3 μs 时, 在第一电离阈以下可观察到明显的收敛于第一电离阈的 Rydberg 能级, 同时在靠近电离阈的位置出现了较宽的自电离峰 (虚线框), 导致第一电离阈并不能明显看到, 而在第一电离阈以上观察到了非常强的共振自电离峰 (*号)。如图 3(b) 所示, 当延时时间增大为 35.8μs 时, 离第一电离阈较远的 Rydberg 原子信号消失, 这是因为与靠近第一电离阈的 Rydberg 态相比, 离第一电离阈较远的 Rydberg 态有着更低的主量子数, 寿命也相对较短, 这样, 在脉冲电场作用时, 这些较低主量子数的 Rydberg 态原子已经跃迁到更低能级而无法被探测到, 这也说明采用延时场电离技术研究 Sm 原子 Rydberg 态时, 延时时间不能过长。对比图 3(a) 和 (c), 可以看到, 在延时时间较短时, 即使存在 0.500 0 V·cm^{-1} 的静电场情况下, 与零场时相比, 自电离信号基本也没有变化。这意味着静电场在如此短的延时下没能将自电离产生的离子推出作用区, 这样, 自电离信号和 Rydberg 信号叠加导致在光谱图中无法直接观测到第一电离阈的位置。在图 3(d) 中, 在仍然存在 0.499 5 V·cm^{-1} 的静电场情况下, 脉冲电场延时时间增大为 35.8 μs。由于延时时间足够长, 在施加

脉冲电场时，静电场已将自电离产生的离子推出作用区而不会被探测到。光谱图中非常强的共振自电离信号完全消失，这样静电场下第一电离阈就可以被直接观测到。

当脉冲电场幅值为 3 000 V·cm^{-1}，t_d 为 35.8 μs 时，得到了在零场和不同强度的静电场下 Sm 原子第一电离阈附近的光谱图，如图 4 所示。*号表示高于第一电离阈非常强的共振自电离态。可以看到，在静电场下，由于消除了自电离和光电离等其它信号的干扰，光谱的信噪比明显提高，同时可以非常清晰地看到第一电离阈，同时，随着电场强度的增强，第一电离阈以下较宽的自电离包络随着电场强度的增强而逐步消失，第一电离阈向低能量有着明显的移动，移动规律遵循公式 (3)。

在 t_d 为 35.8 μs 并施加静电场的条件下，只有第一电离阈以下的 Rydberg 态 Sm 原子的场电离信号被探测到，因此在第一电离阈附近选取信号突然增加位置处的能量作为该静电场下 Sm 原子第一电离阈的位置，如图 5 所示。图 5 中箭头所示位置是静电场强度为 1.999 3 V·cm^{-1} 时 Sm 原子第一电离阈的位置。

通过改变静电场强度可以得到不同静电场下 Sm 原子的第一电离阈的位置，如图 6 所示，图中圆圈表示实验数据，实线表示根据公式 (3) 拟合得到的曲线。图 6(a)、(b)、(c) 中，三步激光 λ_1，λ_2 和 λ_3 的偏振组合分别对应表 1 中的组合 1, 2, 3。

表 2 列出了由不同磁量子数的 Rydberg 态 Sm 原子获得的零场下第一电离阈的拟合结果。从拟合结果可以看出，这些零场下的第一电离阈最大差别仅为 0.49 cm^{-1}。取 3 种组合的平均值 I_0= 45 519.69±0.17 cm^{-1} 为 Sm 原子在零场下的第一电离阈，该值与文献 [6] 得到的数值 45 519.64± 1.39 cm^{-1} 有着很好的一致性，证实了采用电场中电离阈移动的规律获得零场下电离阈的有效性。

4 结 论

本文使用脉冲电场对稀土 Sm 原子的高激发 Rydberg 态进行延时场电离探测，通过在脉冲电场产生之前施加反向静电场和增加延时时间排除了光电离和自电离等其它路径所产生的离子信号的干扰，提高了实验的信噪比。通过改变静电场强度的大小，观察并研究了 Sm 原子第一电离阈随着电场的移动规律。同时通过改变三步激光的偏振组合，精确地确定了不同磁量子数的 Sm 原子零场下的第一电离阈的位置，最后得到 Sm 原子的第一电离阈为 45 519.69±0.17 cm^{-1}，与采用其它方法所确定的值一致，从而验证了该方法的可靠性。

参考文献：

[1] SATO T K, ASAI M, BORSCHEVSKY A, *et al*.. Measurement of the first ionization potential of lawrencium, element 103[J]. *Nature*, 2015, 520(7546): 209-211.

[2] CHHETRI P, ACKERMANN D, BACKE H, *et al*.. Precision measurement of the first ionization potential of nobelium[J]. *Physical Review Letters*, 2018, 120(26): 263003.

[3] RAEDER S, HEGGEN H, TEIGELHÖFER A, *et al*.. Determination of the first ionization energy of polonium by resonance ionization spectroscopy - part I: measurement of even-parity Rydberg states at TRIUMF-ISAC[J]. *Spectrochimica Acta Part B*: *Atomic Spectroscopy*, 2019, 151: 65-71.

[4] BLOCK M. Direct mass measurements and ionization potential measurements of the actinides[J]. *Radiochimica Acta*, 2019, 107(9-11): 821-831.

[5] SHEN X P, WANG W L, ZHAI L H, *et al*.. New spectroscopic data on high-lying excited even-parity levels of atomic neodymium[J]. *Spectrochimica Acta Part B*: *Atomic Spectroscopy*, 2018, 145: 96-98.

[6] JAYASEKHARAN T, RAZVI M A N, BHALE G L. Even-parity bound and autoionizing Rydberg series of the samarium atom[J]. *Journal of Physics B*: *Atomic*, *Molecular and Optical Physics*, 2000, 33(16): 3123-3136.

[7] SCHMITT A, BUSHAW B A, WENDT K. Determination of the ^{154}Sm ionization energy by high-precision laser spectroscopy[J]. *Journal of Physics B*: *Atomic*, *Molecular and Optical Physics*, 2004, 37(8): 1633-1644.

[8] DESCLAUX J P, FRICKE B. Relativistic prediction of the ground state of atomic Lawrencium[J]. *Journal de Physique*, 1980, 41(9): 943-946.

[9] 沈礼, 野仕伟, 戴长建. 电场中Eu原子电离阈移动的实验研究[J]. 物理学报, 2012, 61(6): 063301.
SHEN L, YE SH W, DAI CH J. Experiment study of ionization limit shift of europium atoms in electric fields[J]. *Acta Physics Sinica*, 2012, 61(6): 063301. (in Chinese)

[10] WENDT K, GOTTWALD T, MATTOLAT C, *et al*.. Ionization potentials of the lanthanides and actinides – towards atomic spectroscopy of super-heavy elements[J]. *Hyperfine Interactions*, 2014, 227(1): 55-67.

[11] STUDER D, HEINITZ S, HEINKE R, *et al*.. Atomic transitions and the first ionization potential of promethium determined by laser spectroscopy[J]. *Physical Review A*, 2019, 99(6): 062513.

[12] SHANG X, ZHOU CH X, MA L, *et al*.. The determination of radiative lifetime for some Eu I levels by time-resolved laser-induced fluorescence spectroscopy[J]. *Journal of Quantitative Spectroscopy and Radiative Transfer*, 2019, 224: 103-106.

[13] NIKI H, MOTOKI K, YASUI M, *et al*.. Selectivity and efficiency of laser isotope separation processes of gadolinium[J]. *Journal of Nuclear Science and Technology*, 2006, 43(4): 427-431.

[14] ANG'ONG'A J, GADWAY B. Polarization spectroscopy of atomic erbium in a hollow cathode lamp[J]. *Journal of Physics B*: *Atomic*, *Molecular and Optical Physics*, 2018, 51(4): 045003.

[15] CHHETRI P, MOODLEY C S, RAEDER S, *et al*.. Investigation of the first ionization potential of ytterbium in argon buffer gas[J]. *Acta Physica Polonica B*, 2018, 49(3): 599-603.

[16] GOMONAI A I, REMETA E Y. The effect of field strength on the resonance structure of three-photon ionization spectra of the samarium atom[J]. *Optics and Spectroscopy*, 2013, 114(3): 329-336.

[17] LAWLER J E, FITTANTE A J, DEN HARTOG E A. Atomic transition probabilities of neutral samarium[J]. *Journal of Physics B*: *Atomic*, *Molecular and Optical Physics*, 2013, 46(21): 215004.

[18] SEEMA A U, MANDAL P K, SAHOO A C, *et al*.. Radiative lifetimes of even-parity high-lying levels of Sm I by delayed photoionization measurements[J]. *Journal of Quantitative Spectroscopy and Radiative Transfer*, 2018, 216: 1-5.

[19] SAHOO A C, MANDAL P K, SHAH M L, *et al*.. Enhancement of photoionization by applying polarization-based common level excitation scheme for the selective photoionization of odd isotopes of samarium[J]. *Journal of Quantitative Spectroscopy and Radiative Transfer*, 2019, 235: 7-14.

[20] WU B R, XU Y F, ZHENG Y F, *et al*.. An experimental investigation of the autoionizing levels of neutral ytterbium[J]. *Journal of Physics B*: *Atomic*, *Molecular and Optical Physics*, 1992, 25(2): 355-361.

[21] WORDEN E F, SOLARZ R W, PAISNER J A *et al*.. First ionization potentials of lanthanides by laser spectroscopy[J]. *Journal of the Optical Society of America*, 1978, 68(1): 52-61.

[22] LÜ J, DAI CH J, XU Y F, *et al*.. Perturbed 6snd $^{1,3}D_2$ rydberg series of neutral barium[J]. *Chinese Physics Letters*, 2001, 18(9): 1192-1195.

[23] 李庆运, 花磊, 何梦琦, 等. 高气压光电离-化学电离-飞行时间质谱在绿茶香型快速鉴别中的应用[J]. 分析化学, 2019, 47(4): 541-549.
LI Q Y, HUA L, HE M Q, *et al*.. High-pressure photoionization/chemical ionization-time-of-flight mass spectrometry for classification and identification of green tea aromas[J]. *Chinese Journal of Analytical Chemistry*, 2019, 47(4): 541-549. (in Chinese)

[24] 何梦琦, 花磊, 李庆运, 等. 甲苯增强高气压光电离-飞行时间质谱高灵敏快速测量酚类化合物[J]. 分析化学, 2019, 47(3): 447-454.
HE M Q, HUA L, LI Q Y, *et al*.. Toluene enhanced-high pressure photoionization-time-of-flight mass spectrometry for highly sensitive and rapid detection of phenolic compounds[J]. *Chinese Journal of Analytical Chemistry*, 2019, 47(3): 447-454. (in Chinese)

[25] MARTIN W C, ZALUBAS R, HAGAN L. *Atomic Energy Levels*, *The Rare-Earth Elements*[M]. Washington: National Bureau of Standards, 1978.

[26] 朱红求, 周涛, 李勇刚, 等. 基于提升建模的锌离子与钴离子浓度紫外可见吸收光谱检测方法[J]. 分析化学, 2019, 47(4): 576-582.

ZHU H Q, ZHOU T, LI Y G, *et al*.. An ultraviolet-visible absorption spectrometric method for detection of zinc (Ⅱ) and cobalt (Ⅱ) ions concentration based on boosting modeling[J]. *Chinese Journal of Analytical Chemistry*, 2019, 47(4): 576-582. (in Chinese)

[27] 曾坤, 马源源, 郭庆中, 等. 电感耦合等离子发射光谱法快速测定对苯二甲酰氯中氯化亚砜残留量[J]. 分析化学, 2019, 47(3): 410-414.
ZENG K, MA Y Y, GUO Q ZH, *et al*.. Determination of thionyl chloride residue in terephthaloyl chloride by inductively coupled plasma-optical emission spectrometry[J]. *Chinese Journal of Analytical Chemistry*, 2019, 47(3): 410-414. (in Chinese)

[28] DAI CH J, ZHANG S, SHU X W, *et al*.. Pulsed electric-field ionization of Stark states of neutral ytterbium[J]. *Journal of Quantitative Spectroscopy and Radiative Transfer*, 1995, 53(2): 179-188.

[29] ELIZAROV A Y, CHEREPKOV N A. Two-photon polarization spectroscopy of autoionizing states[J]. *Soviet Physics - JETP*, 1989, 69(4): 695-699.

Author Biographics:

Xu Zhaojin (1978—), male, born in Minhou, Fujian. He is an associate professor with a master's degree. In 2005, he received his master's degree from Nankai University. Now he is an associate professor of the School of Science, Tianjin University of Technology, mainly engaged in the research of spectroscopy and its application. E-mail: xuzhaojin1234@126.com

许照锦(1978—), 男, 福建闽侯人, 硕士, 副教授, 2005 年于南开大学获得硕士学位, 现为天津理工大学理学院副教授, 主要从事光谱学与应用研究。E-mail: xuzhaojin1234@126.com

Shen Li (1982—), male, born in Wuhan, Hubei. He is an associate professor with a doctorate. In 2009, he received his PhD from the Wuhan Institute of Physics and Mathematics, Chinese Academy of Sciences. Now he is an associate professor of the School of Science, Tianjin University of Technology, mainly engaged in the research of spectroscopy and its application. E-mail: shenli@tjut.edu.cn

沈　礼(1982—), 男, 湖北武汉人, 博士, 副教授, 2009 年于中国科学院武汉物理与数学研究所获得博士学位, 现为天津理工大学理学院副教授, 主要从事光谱学与应用研究。E-mail: shenli@tjut.edu.cn